WILLETT, R. D. (1988). *Acta Cryst.* B44, 503–508.
WILLETT, R. D., BOND, M. R., HAIJE, W. E., SOONIEUS, O. P. M. & MAASKANT, W. J. A. (1988). *Inorg. Chem.* 27, 614–620.
WILLETT, R. D., BOND, M. R. & PON, G. (1990). *Inorg. Chem.* 29, 4160–4162.
WILLETT, R. D. & GEISER, U. (1986). *Inorg. Chem.* 25, 4558–4561.
WILLETT, R. D., GRIGEREIT, T., HALVORSON, K. & SCOTT, B. (1987). *Indian Acad. Sci.* 98, 147–160.
WILLETT, R. D., PLACE, H. & MIDDLETON, M. (1988). *J. Am. Chem. Soc.* 110, 8639–8650.
WILLETT, R. D. & RUNDLE, R. E. (1964). *J. Chem. Phys.* 40, 838–847.

Acta Cryst. (1993). B49, 289–303

Structures of Hexakis(1-propyltetrazole)iron(II) Bis(tetrafluoroborate), $[Fe(CHN_4C_3H_7)_6](BF_4)_2$, Hexakis(1-methyltetrazole)iron(II) Bis(tetrafluoroborate), $[Fe(CHN_4CH_3)_6](BF_4)_2$, and the Analogous Perchlorates. Their Relation to Spin Crossover Behaviour and Comparison of Debye–Waller Factors from Structure Determination and Mössbauer Spectroscopy

BY LEONORE WIEHL

Mineralogisches Institut der Universität Bonn, Poppelsdorfer Schloß, 5300 Bonn 1, Germany

(*Received* 14 *December* 1991; *accepted* 24 *August* 1992)

Abstract

Single-crystal structure determinations of the spin crossover compounds $[Fe(ptz)_6]X_2$ and $[Fe(mtz)_6]X_2$ (ptz = $C_3H_7N_4CH$, mtz = CH_3N_4CH, $X = BF_4$, ClO_4) have been performed at different temperatures. The temperature dependence of the lattice constants was measured for the two mtz compounds between 300 and 110 K. The two different structure types for the ptz and mtz compounds are compared and discussed in relation to the physical properties associated with the temperature-induced and light-induced spin transitions. In particular, the atomic displacement parameters for the two inequivalent Fe complexes in the mtz structure were found to be significantly different. They are in good accordance with the vibrational amplitudes derived from the Debye–Waller factors measured by Mössbauer spectroscopy. Crystal data, measured with Mo $K\alpha$ radiation, $\lambda = 0.71069$ Å: (*S*1) $[Fe(ptz)_6](ClO_4)_2$ at 299 K: $M_r = 927.6$, $R\bar{3}$ ($Z = 3$), D_m (295 K) = 1.33, $D_x = 1.333$ Mg m^{-3}, $a = 10.804$ (3), $c = 34.296$ (5) Å, $V = 3467$ (1) Å^3, $F(000) = 1446$, $\mu = 0.461$ mm^{-1}, $R = 0.115$ (1965 unique reflections), isostructural to (*S*2). (*S*2) $[Fe(ptz)_6](BF_4)_2$ at 297, 250 and 195 K: $M_r = 902.3$, $R\bar{3}$ ($Z = 3$), D_m (295 K) = 1.32, $D_x = 1.312$ Mg m^{-3}, $a = 10.833$ (2), $c = 33.704$ (6) Å, $V = 3425$ (1) Å^3 at 297 K, $a = 10.857$ (3), $c = 33.053$ (13) Å, $V = 3374$ Å^3 at 250 K and $a = 10.890$ (2), $c = 32.330$ (10) Å, $V = 3320$ (1) Å^3 at 195 K; $F(000) = 1398$; $\mu = 0.368$ mm^{-1} (297 K), 0.373 mm^{-1} (250 K) and 0.380 mm^{-1} (195 K); $R = 0.125$ (2058 unique reflections) at 297 K, $R = 0.114$ (1799 unique reflections) at 250 K and $R = 0.077$ (1695 unique reflections) at 195 K. (*S*3) $[Fe(mtz)_6](ClO_4)_2$ at 298 K: $M_r = 759.2$, $P2_1/n$ ($Z = 4$), $D_m = 1.55$, $D_x = 1.551$ Mg m^{-3}, $a = 18.270$ (4), $b = 10.367$ (2), $c = 18.674$ (5) Å, $\beta = 113.16$ (2)°, $V = 3252$ (1) Å^3, $F(000) = 1544$, $\mu = 0.647$ mm^{-1}, $R = 0.083$ (4529 unique reflections), isostructural to (*S*4). (*S*4) $[Fe(mtz)_6](BF_4)_2$ at 157 and 113 K: $M_r = 733.9$, $P2_1/n$ ($Z = 4$), $D_m = 1.53$, $D_x = 1.524$ Mg m^{-3} at 295 K; $a = 17.778$ (6), $b = 10.215$ (2), $c = 18.625$ (6) Å, $\beta = 114.03$ (2)°, $V = 3089$ (2) Å^3 at 157 K and $a = 17.673$ (7), $b = 10.178$ (5), $c = 18.648$ (8) Å, $\beta = 114.27$ (3)°, $V = 3058$ (2) Å^3 at 113 K; $F(000) = 1480$; $\mu = 0.535$ mm^{-1} (157 K) and 0.540 mm^{-1} (113 K); $R = 0.090$ (4485 unique reflections) at 157 K and $R = 0.074$ (4625 unique reflections) at 113 K.

Introduction

The tetrazole compounds of type $[Fe(R\text{-tz})_6]X_2$ (*R*-tz = 1-alkyltetrazole, $X = BF_4$, ClO_4, PF_6, CF_3SO_3) belong to the large group of octahedrally coordinated Fe^{2+} spin crossover compounds, which undergo a transition from the high-spin (HS) state ($^5T_2$) to the low-spin (LS) state ($^1A_1$) on cooling. HS $\rightarrow$LS transitions are accompanied by a contraction of the Fe—ligand bond distances of up to 0.2 Å (see review of X-ray structures: König, 1987), leading to elastic interactions between large HS and small LS molecules in the transition region (Spiering, Meissner, Köppen, Müller & Gütlich, 1982; Adler,

0108-7681/93/020289-15$06.00

Wiehl, Meissner, Köhler, Spiering & Gütlich, 1987; Willenbacher & Spiering, 1988; Spiering & Willenbacher, 1989) and resulting in a decrease of lattice constants in the order of per cent (Meissner, Köppen, Spiering & Gütlich, 1983; Wiehl, Kiel, Köhler, Spiering & Gütlich, 1986). There may or may not be a structural phase transition too, but in each case there is a high interdependence of crystal structure and spin transition features.

The spin transition behaviour of the tetrazole compounds has been extensively investigated by Mössbauer spectroscopy, optical spectroscopy (UV–visible) and measurements of magnetic susceptibility and of heat capacity. The crystal structure work presented here, which proceeded parallel to these measurements, added essential information for their interpretation. Most of the results are published elsewhere (referenced later on), the most recent papers already anticipating the knowledge of some structural details.

Many tetrazole compounds were first synthesized by Franke (Franke, Haasnoot & Zuur, 1982; Franke, 1982). From powder diffractograms he concluded that several different structure types were present. Our interest in these compounds arose from the discovery of the LIESST (light-induced excited spin state trapping) effect in $[Fe(ptz)_6](BF_4)_2$ (*S*2) (ptz = 1-propyltetrazole) by Decurtins and Hauser (Decurtins, Gütlich, Köhler, Spiering & Hauser, 1984). This effect means the excitation of a long-lived (order of days) metastable high-spin state by irradiating the crystal with light of suitable wavelength at temperatures well below the normal (= temperature-induced) spin transition, where the low spin is the thermodynamically stable state. Light-induced high-spin states were later found for several other substances (Decurtins, Gütlich, Köhler & Spiering, 1985; Decurtins, Gütlich, Hasselbach, Hauser & Spiering, 1985; Poganiuch & Gütlich, 1987) and the phenomenon seems to be a general feature of spin crossover compounds.

X-ray powder diffraction of $[Fe(ptz)_6](BF_4)_2$ (*S*2) in the range from room temperature to 10 K (Wiehl, Spiering, Gütlich & Knorr, 1990) showed that the transition from HS to LS at about 130 K is accompanied by a displacive structural phase transition with a very sharp decrease of the lattice constants. The light-induced transition from LS to HS below 50 K, however, does not restore the HS crystal structure, as has been proven by the powder measurements at that temperature. The knowledge of the HS crystal structure is essential for understanding these results.

A structure determination of $[Fe(ptz)_6](BF_4)_2$ (*S*2) had already been tried by Franke (1982). At room temperature the evaluation of data failed completely, and at 140 K a reliability of only ~20% for isotropic refinement (space group $R\bar{3}$, $Z = 3$) was achieved. The difficulties in the latter case were attributed to an appreciable amount of small LS molecules in the crystal starting the spin transition. Comparison of lattice parameters from the powder data mentioned above with magnetic susceptibility data (Decurtins, Gütlich, Hasselbach, Hauser & Spiering, 1985), however, yields an LS fraction of only ~5% at 140 K. So the proposed disorder of HS and LS molecules is not likely to be a serious problem. Moreover, Mössbauer spectra measured with crystal samples from Franke showed an additional peak due to impurities (Müller, Ensling, Spiering & Gütlich, 1983). This confirmed our expectation that his problems with the structure were merely a question of poor crystal quality and could be overcome by better preparation.

A new crystal structure and new properties arise in the 1-alkyltetrazole compounds when changing the propyl group into methyl. Mössbauer spectroscopy of $[Fe(mtz)_6]X_2$ [$X = BF_4$ (*S*4), ClO_4 (*S*3)] (Poganiuch, Decurtins & Gütlich, 1990; Poganiuch & Gütlich, 1988) exhibits two different HS states with significantly different Debye–Waller factors, only one of them undergoing the spin transition at 75 K [BF_4, (S4)] and 66 K [ClO_4, (*S*3)]. Nevertheless, the second HS state can be converted to LS too by irradiation with light below 55 K in both compounds. In these substances [(*S*3), (*S*4)] the main question concerns the structural differences of the two HS complexes and why only one of them is capable of a normal (*i.e.* temperature-induced) spin transition. Of special interest in this connection is the comparison with the distinct structure of the chemically closely related propyltetrazoles [(*S*1), (*S*2)].

Additionally, comparison of atomic displacement parameters with Debye–Waller factors from Mössbauer measurements provides a means of testing the reliability of the so-called 'temperature factors'.

Chemical preparation and crystal characterization

For the synthesis of $[Fe(R\text{-tz})_6]X_2$ (*R*-tz = 1-alkyltetrazole, $R = CH_3$, C_3H_7, tz = N_4CH, $X = BF_4$, ClO_4) a method of Kamiya & Saito (1971) and Franke & Groeneveld (1981) was optimized by Poganiuch (1989), which resulted in chemically pure compounds and, after recrystallization from nitromethane, in crystals of good quality with reproducible properties (checked especially by Mössbauer spectroscopy and magnetic susceptibility measurements). The density was measured for a number of crystal samples of about 1 mm size by the flotation method in a mixture of petroleum ether and carbon tetrachloride.

All compounds crystallize as colourless plates with a good cleavage in the plane of the plates. In the case

Table 1. *Data collection and refinement of the propyltetrazoles*

	$[Fe(ptz)_6](ClO_4)_2$ (*S*1)	$[Fe(ptz)_6](BF_4)_2$ (*S*2) Crystal 1	Crystal 2*	
Temperature (K)	299	297	250	195
Hexagonal plates (mm)	1.3 × 1.0 × 0.25	0.78 × 0.81 × 0.25	0.44 × 0.36 × 0.12	
Maximum $(\sin\theta)/\lambda$ (Å^{-1})	0.746	0.807	0.682	0.661
Range of h, k, l	$0 \le (h, k) \le 16$, $-48 \le l \le 48$	$0 \le (h, k) \le 17$, $-54 \le l \le 54$	$0 \le h \le 14$, $-14 \le k \le 14$, $-17 \le l \le 17$	$-16 \le l \le 16$
Standard reflections	511, 34$\bar{4}$, $\bar{4}$,0,$\bar{16}$	511, 34$\bar{4}$, 4,0,16	257, $\bar{7}$3$\bar{4}$, 564	
with intensity loss (%)	0.4	3.7	4.2	2.4
Measured reflections	3024	3795	6301	5607
R_{int}	0.025	0.022	0.028	0.033
Unique reflections $[I > 0.5\sigma(I)]$	1965	2058	1799	1695
Unobserved reflections	780	1461	1166	606
Parameters refined; data/parameter ratio	117; 16.8	118; 17.4	103; 17.5	103; 16.5
Values of R, wR	0.115/0.104	0.125/0.108	0.114/0.105	0.077/0.092
ε (used in weights)	0.007	0.006	0.008	0.023
$(\Delta/\sigma)_{max}$	0.008	0.30 (F: 1.32)	0.003	0.010
Max./min. $\Delta\rho$ (e Å^{-3})	0.519/−1.239	0.393/−1.545	1.47/−0.89	1.33/−0.61

*hkl referred to triclinic axes.

of the propyltetrazole (ptz) compounds [(*S*1), (*S*2)] the hexagonal plates are optically uniaxial. The methyltetrazole (mtz) crystals [(*S*3), (*S*4)] show pseudohexagonal plates, which are optically biaxial with the acute bisectrix perpendicular to the plates. The crystals are very soft and in the case of mtz–ClO_4, some thin plates were already bent on growing. It was impossible to cut crystals into smaller pieces without introducing many defects; in the diffraction patterns of such pieces (oscillation photographs on the diffractometer) the peaks were smeared out along the Debye–Scherrer circles. Thus it was inevitable that one had to use rather large crystals for the structure determination in some cases where crystals grown with a suitable diameter were by far too thin to give enough diffracted intensity.

The space groups of the four compounds were determined from Weissenberg and precession photographs at room temperature: $R\bar{3}$ (No. 148, $Z = 3$ for the hexagonal setting) for $[Fe(ptz)_6]X_2$ [$X = BF_4$ (*S*2), ClO_4 (*S*1)] and $P2_1/n$ (standard setting $P2_1/c$, No. 14, $Z = 4$) for $[Fe(mtz)_6]X_2$ [$X = BF_4$ (*S*4), ClO_4 (*S*3)] showing the following absences: $0k0$ with $k \neq 2n$ and $h0l$ with $h + l \neq 2n$. The monoclinic axis is in the plane of the crystal plates.

Structure determination: measurements

All intensity data were collected on a four-circle diffractometer (Enraf–Nonius CAD-4) with Mo $K\alpha$ radiation ($\lambda = 0.71069$ Å, graphite monochromator), using ω–2θ scans. For the low-temperature measurements the crystal was cooled by a cold gas stream produced by evaporation of liquid nitrogen. The temperature was kept constant within 0.1 K by a PID controller (device: Enraf–Nonius). The temperature scale was calibrated using a copper isotan thermocouple in place of the crystal. The thermocouple was made from extremely fine wires with the first few centimetres wound to a small spiral and fully inserted in the cold gas stream in order to avoid errors produced by heat transport.

(*a*) Propyltetrazole compounds: single-crystal structure determinations were performed for $[Fe(ptz)_6](ClO_4)_2$ (*S*1) at 299 K and for the isostructural $[Fe(ptz)_6](BF_4)_2$ (*S*2) at 297 K (crystal 1) and at 250 and 195 K (crystal 2). Data-collection parameters are given in Table 1. The lattice parameters were calculated from the setting angles of 25 reflections in the range $12 < \theta < 15°$. The temperature dependence of the lattice constants of $[Fe(ptz)_6](BF_4)_2$ (*S*2) (as measured on the four-circle diffractometer in the range 300 to ~170 K) reproduced the values measured earlier with a powder sample (Wiehl, Spiering, Gütlich & Knorr, 1990). Thus these are not reported here. In contrast to expectation, however, it was not possible to extend the lattice-constant measurements down to the transition temperature of 130 K. Several crystal samples were tried, but intensities faded during cooling at varying temperatures some 10 K above the transition. Furthermore, the intensities of equivalent reflections due to the threefold axis showed increasing differences in the lower temperature region (just before fading). One crystal was broken at 190 K, indicated by the splitting of peaks in a polaroid photograph. So the suspicion arose that there could be another phase transition. In order to check the threefold symmetry, two structure determinations with a second crystal at 250 and 195 K were made using the primitive unit cell along $[100]_H$, $[110]_H$ and $[\bar{2}\bar{1}\bar{1}/\bar{3}\bar{3}\bar{3}]_H$ (space group $P\bar{1}$, $Z = 1$) with $a = 10.859$ (4), $b = 10.850$ (6), $c = 12.676$ (4) Å, $\alpha = 64.65$ (4), $\beta = 64.65$ (3), $\gamma = 60.04$ (4)° ($T = 250$ K) and $a = 10.888$ (3), $b = 10.886$ (3), $c = 12.476$ (4) Å, $\alpha = 64.16$ (3), $\beta = 64.12$ (2), $\gamma = 60.05$ (2)° ($T = 195$ K). The data were later merged in space group $R\bar{3}$ with the result that the threefold axis was confirmed.

Table 2. *Data collection and refinement of the methyltetrazoles*

	$[Fe(mtz)_6](ClO_4)_2$ (*S*3)	$[Fe(mtz)_6](BF_4)_2$ (*S*4)	
Temperature (K)	298	157	113
Pseudohexagonal plates (mm)	0.60 × 0.39 × 0.28	0.25 × 0.14 × 0.09	
Maximum $(\sin\theta)/\lambda$ (Å^{-1})	0.682	0.661	
Range of h, k, l	$0 \le h \le 24, 0 \le k \le 14, -25 \le l \le 25$	$0 \le h \le 23, 0 \le k \le 13, -24 \le l \le 24$	
Standard reflections	080, 6,4,$\bar{1}2$, $\bar{8}66$	5$\bar{1}2$, 4,0,$\bar{1}2$, 431	
with intensity loss (%)	3	2.9	3.8
Measured reflections	9383	8104	8027
R_{int}	0.020	0.033	0.027
Unique reflections	4529 [$I > 2\sigma(I)$]	4485 [$I > 0.5\sigma(I)$]	4625 [$I > 0.5\sigma(I)$]
Unobserved reflections	4624	3444	3216
Parameters refined; data/parameter ratio	465; 9.7	465; 9.6	465; 9.9
Values of R, wR	0.83/0.101	0.090/0.070	0.074/0.060
ε (used in weights)	0.023	0.0205	0.0195
$(\Delta/\sigma)_{max}$	0.11	0.05	0.04
Max./min. $\Delta\rho$ (e Å^{-3})	1.36/−0.67	1.06/−0.95	0.70/−0.95

(*b*) Methyltetrazole compounds: intensity data were collected for $[Fe(mtz)_6](ClO_4)_2$ (*S*3) at 298 K and for the isostructural $[Fe(mtz)_6](BF_4)_2$ (*S*4) at 157 and 113 K. Data-collection parameters are given in Table 2. The lattice parameters were calculated from the setting angles of 25 reflections in the ranges $14 < \theta < 16°$ (ClO_4) and $6 < \theta < 13°$ (BF_4). Furthermore, the temperature dependence of the lattice constants was measured on the four-circle diffractometer in 15 K steps in the temperature range $295 > T > 160$ K [ClO_4, (*S*3), Fig. 1] and $270 > T > 110$ K [BF_4, (*S*4), Fig. 2)] (data included in the supplementary material). The latter sample was mounted with a less strong adhesive, vacuum grease, which was too soft at room temperature. For the tetrafluoroborate (*S*4) all measurements were made with the same crystal sample. The perchlorate crystals (*S*3), however, cracked on cooling at various temperatures and the lattice constants as functions of temperature stem from two different crystal samples. It was impossible to extend the measurements below 160 K or to collect a complete set of intensity data below room temperature, though many crystal samples were tried. The perchlorate crystals could not be prepared in the same good quality as the tetrafluoroborates in spite of the same method of chemical synthesis and technique of crystal growing.

Structure determination: calculations

The intensities were Lp and decay corrected. No absorption correction was applied, as the absorption

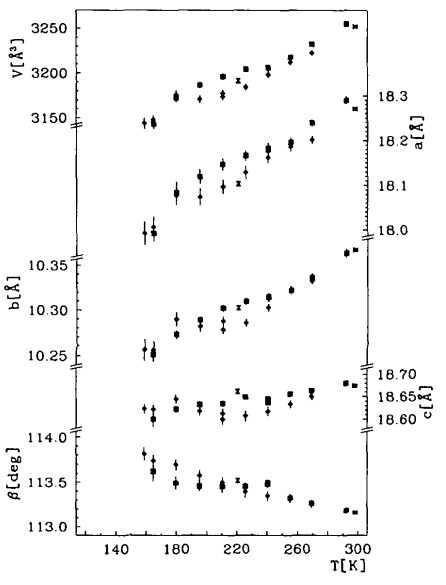

Fig. 1. Temperature dependence of lattice parameters of $[Fe(mtz)_6](ClO_4)_2$ (*S*3). The different symbols refer to different crystal samples.

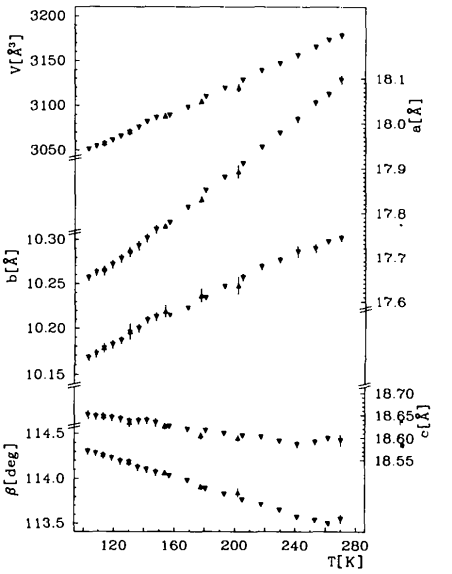

Fig. 2. Temperature dependence of lattice parameters of $[Fe(mtz)_6](BF_4)_2$ (*S*4). The triangles pointing down and up indicate data measured on cooling and heating with the same crystal sample.

Table 3. *Atomic positional and equivalent isotropic displacement parameters of* $[Fe(ptz)_6](ClO_4)_2$ (*S*1) *at* 299 K *and* $[Fe(ptz)_6](BF_4)_2$ (*S*2) *at* 297, 250 *and* 195 K

$U_{eq} = (1/3)\sum_i \sum_j U_{ij} a_i^* a_j^* \mathbf{a}_i . \mathbf{a}_j .$

	x	*y*	*z*	*U* (Å²)
$[Fe(ptz)_6](ClO_4)_2$ (*S*1) at 299 K				
Fe1	0.0	0.0	0.0	0.0592 (5)
N4	0.0608 (3)	0.8747 (3)	0.0361 (1)	0.0712 (17)
N3	0.1651 (4)	0.9300 (4)	0.0637 (1)	0.1018 (23)
N2	0.1687 (5)	0.8307 (5)	0.0836 (1)	0.1058 (24)
N1	0.0659 (4)	0.7077 (4)	0.0689 (1)	0.0770 (18)
Cl	−0.0009 (4)	0.7334 (4)	0.0398 (1)	0.0714 (21)
C2	0.0417 (7)	0.5680 (6)	0.0840 (2)	0.1091 (34)
C3	−0.0003 (15)	0.5409 (11)	0.1225 (3)	0.2012 (93)
C4	−0.1048 (13)	0.5566 (11)	0.1372 (3)	0.2093 (91)
Cl1	0.0	0.0	0.3255 (1)	0.0836 (8)
O1*a*	0.0	0.0	0.2853 (1)	0.207 (12)
O2*a*	−0.0315 (25)	0.1013 (18)	0.3388 (1)	0.257 (17)
O1*b*	0.0	0.0	0.3656 (1)	0.199 (11)
O2*b*	0.1255 (7)	0.1145 (9)	0.3122 (1)	0.147 (6)
$[Fe(ptz)_6](BF_4)_2$ (*S*2) at 250 K				
Fe1	0.0	0.0	0.0	0.0399 (6)
N4	0.0527 (4)	0.08688 (4)	0.0376 (1)	0.0464 (18)
N3	0.1608 (4)	0.9219 (4)	0.0649 (1)	0.0685 (23)
N2	0.1649 (5)	0.8186 (5)	0.0836 (1)	0.0709 (24)
N1	0.0593 (4)	0.6987 (4)	0.0685 (1)	0.0516 (20)
C1	−0.0084 (5)	0.7295 (5)	0.0404 (1)	0.0494 (24)
C2	0.0353 (7)	0.5560 (6)	0.0815 (2)	0.0733 (32)
C3	0.0041 (10)	0.5346 (8)	0.1254 (2)	0.1200 (55)
C4	−0.1144 (10)	0.5438 (10)	0.1410 (3)	0.1369 (62)
B1	0.0	0.0	0.3238 (4)	0.0626 (42)
F1	0.0	0.0	0.2842 (3)	0.2598 (83)
F2	−0.0504 (6)	−0.1299 (5)	0.3274 (2)	0.2146 (42)

	x	*y*	*z'*	*U* (Å²)
$[Fe(ptz)_6](BF_4)_2$ (*S*2) at 297 K				
Fe1	0.0	0.0	0.0	0.0459 (6)
N4	0.0540 (4)	0.8697 (4)	0.0372 (1)	0.0559 (19)
N3	0.1614 (4)	0.9250 (4)	0.0642 (1)	0.0824 (24)
N2	0.1646 (5)	0.8222 (5)	0.0831 (1)	0.0854 (26)
N1	0.0606 (4)	0.7000 (4)	0.0681 (1)	0.0618 (21)
Cl	−0.0062 (5)	0.7300 (5)	0.0404 (1)	0.0586 (25)
C2	0.0370 (7)	0.5586 (6)	0.0820 (2)	0.0918 (35)
C3	−0.0024 (14)	0.5337 (10)	0.1245 (3)	0.1857 (87)
C4	−0.1120 (13)	0.5484 (11)	0.1396 (3)	0.1907 (84)
B1	0.0	0.0	0.3244 (2)	0.0775 (45)
F1*a*	0.0	0.0	0.2854 (2)	0.180 (11)
F2*a*	−0.0455 (15)	0.0845 (14)	0.3373 (2)	0.177 (11)
F1*b*	0.0	0.0	0.3633 (2)	0.195 (14)
F2*b*	0.1230 (6)	0.1028 (11)	0.3115 (2)	0.163 (9)
$[Fe(ptz)_6](BF_4)_2$ (*S*2) at 195 K				
Fe1	0.0	0.0	0.0	0.0285 (3)
N4	0.0503 (3)	0.8669 (3)	0.0386 (1)	0.0342 (10)
N3	0.1606 (3)	0.9184 (3)	0.0655 (1)	0.0492 (13)
N2	0.1644 (3)	0.8151 (3)	0.0834 (1)	0.0513 (13)
N1	0.0573 (3)	0.6955 (3)	0.0687 (1)	0.0367 (11)
C1	−0.0113 (3)	0.7282 (3)	0.0410 (1)	0.0370 (13)
C2	0.0331 (4)	0.5540 (4)	0.0811 (1)	0.0502 (17)
C3	0.0033 (5)	0.5303 (5)	0.1272 (1)	0.0655 (22)
C4	−0.1212 (6)	0.5366 (6)	0.1406 (2)	0.0849 (29)
B1	0.0	0.0	0.3224 (2)	0.0426 (19)
F1	0.0	0.0	0.2796 (2)	0.1742 (41)
F2	−0.0813 (4)	0.0534 (4)	0.3312 (1)	0.1452 (28)

coefficients of $\sim 0.4\ mm^{-1}$ are sufficiently small to be negligible. Nevertheless, an influence could not be ruled out beforehand because of the platy habit of the crystals. So an absorption correction was calculated for one of the compounds [(*S*2) at 297 K], but the final *R*, *wR* values were improved only by 0.001, which is not significant. In least-squares calculations *F* values were used with weights of the form $w = [\sigma^2(F) + (\varepsilon/2)^2 F^2]^{-1/2}$, where ε is the relative error of intensities due to instrumental instability and has been derived from the scattering of standard reflections about their regression curve (McCandlish, Stout & Andrews, 1975). Scattering factors were taken from Doyle & Turner (1968) for Fe^{2+} and from Cromer & Mann (1968) for all other atoms. Anomalous-scattering factors were included from Cromer & Liberman (1970). All structure calculations were performed with the program *SHELX*76 (Sheldrick, 1976) and the thermal ellipsoid plots made with *ORTEP* (Johnson, 1966). Bond distances and angles were calculated with *ORFFE* (Busing, Martin & Levy, 1964).

(*a*) Propyltetrazole compounds [(*S*1), (*S*2)]: With Fe at 0,0,0 the structure could be solved by Fourier syntheses of the electron density distribution. All non-H atoms were refined anisotropically. Fe was fixed at 0,0,0 (site symmetry $\bar{3}$) and B/Cl and F1/Cl1 were fixed to lie on the threefold axis. The anionic BF_4 (*S*2) and ClO_4 (*S*1) groups are disordered and the appropriate model is probably a rotational oscillation. This may be approximated with the *SHELX* program only by splitting the anion position into several different orientations. At room temperature the strongest difference electron density peaks for F/O belonged to two different orientations of the group with one B—F/Cl—O bond 'up' and 'down' along the threefold axis. The F/O positions were constrained to build up two regular tetrahedra with one common B/Cl at the centre. For the anisotropic displacement parameters (ADP's) of the atoms no additional constraints were introduced. Only one common B—F/Cl—O distance was refined and the site occupation factors $a:b = x:(1-x)$ of the two groups resulted in $x = 0.56\ (2)$ for the BF_4 compound (*S*2) at 298 K. For the ClO_4 compound [(*S*1), 299 K] the parameter x did not refine to a stable value and was fixed to $x = 0.5$. The large ADP's of F/O and the new difference density peaks between the F/O positions, however, indicated that these two orientations are not a satisfying model of the anion disorder. Introduction of more different orientations means the introduction of a large number of physically meaningless parameters. So it seemed to be better to refine only one anion orientation, whenever possible, instead of an inadequate model for disorder. Only at room temperature were the difference electron density peaks so similar in strength for the two different orientations that no decision was pos-

Table 4. *Atomic positional and equivalent isotropic displacement parameters of* $[Fe(mtz)_6](ClO_4)_2$ (*S3*) at 298 K

	x	*y*	*z*	*U* (Å²)
Fe1	0.0	0.0	0.0	0.0385 (4)
N411	0.0684 (3)	0.1200 (4)	−0.0456 (3)	0.0427 (20)
N311	0.1327 (3)	0.1907 (6)	0.0004 (3)	0.0619 (26)
N211	0.1714 (4)	0.2280 (6)	−0.0392 (4)	0.0736 (30)
N111	0.1327 (3)	0.1858 (5)	−0.1123 (3)	0.0543 (24)
C111	0.0705 (4)	0.1192 (6)	−0.1153 (4)	0.0492 (27)
C211	0.1594 (6)	0.2170 (10)	−0.1741 (5)	0.0954 (47)
N421	−0.0758 (3)	0.1638 (5)	0.0012 (3)	0.0473 (21)
N321	−0.1266 (4)	0.1622 (6)	0.0373 (3)	0.0695 (31)
N221	−0.1678 (4)	0.2677 (6)	0.0226 (4)	0.0725 (31)
N121	−0.1440 (3)	0.3378 (5)	−0.0251 (3)	0.0536 (23)
C121	−0.0884 (4)	0.2745 (6)	−0.0376 (4)	0.0546 (30)
C221	−0.1766 (5)	0.4682 (6)	−0.0513 (5)	0.0816 (38)
N431	0.0810 (3)	0.0467 (5)	0.1206 (3)	0.0427 (19)
N331	0.1372 (3)	−0.0334 (5)	0.1680 (3)	0.0567 (23)
N231	0.1824 (3)	0.0254 (6)	0.2306 (3)	0.0623 (25)
N131	0.1553 (3)	0.1471 (5)	0.2239 (3)	0.0475 (21)
C131	0.0945 (4)	0.1589 (6)	0.1573 (3)	0.0478 (26)
C231	0.1935 (5)	0.2413 (7)	0.2865 (4)	0.0721 (33)
Fe2	0.5	0.0	0.0	0.0604 (6)
N412	0.4348 (3)	0.1255 (6)	−0.0981 (3)	0.0617 (27)
N312	0.3787 (4)	0.2078 (7)	−0.0993 (4)	0.0836 (36)
N212	0.3472 (4)	0.2644 (8)	−0.1665 (4)	0.0912 (37)
N112	0.3837 (3)	0.2216 (6)	−0.2091 (3)	0.0611 (26)
C112	0.4368 (5)	0.1370 (8)	−0.1682 (4)	0.0721 (38)
C212	0.3663 (6)	0.2705 (10)	−0.2876 (4)	0.0938 (45)
N422	0.5713 (4)	0.1644 (6)	0.0618 (3)	0.0623 (27)
N322	0.6175 (5)	0.1657 (8)	0.1371 (4)	0.0913 (37)
N222	0.6621 (5)	0.2658 (8)	0.1538 (4)	0.1046 (41)
N122	0.6434 (4)	0.3360 (6)	0.0893 (4)	0.0645 (28)
C122	0.5887 (5)	0.2727 (8)	0.0347 (4)	0.0764 (40)
C222	0.6833 (6)	0.4554 (8)	0.0874 (6)	0.0982 (49)
N432	0.4144 (4)	0.0380 (6)	0.0523 (3)	0.0652 (29)
N332	0.3615 (5)	−0.0483 (7)	0.0578 (4)	0.0925 (40)
N232	0.3205 (4)	−0.0018 (7)	0.0928 (5)	0.0929 (40)
N132	0.3455 (3)	0.1187 (6)	0.1113 (3)	0.0567 (25)
C132	0.4023 (5)	0.1411 (8)	0.0871 (5)	0.0724 (39)
C232	0.3115 (4)	0.2029 (8)	0.1542 (4)	0.0724 (36)
Cl1	0.4576 (1)	0.5050 (2)	0.1497 (1)	0.0726 (9)
O11	0.3793 (5)	0.4796 (8)	0.0992 (5)	0.164 (5)
O21	0.4582 (7)	0.6175 (14)	0.1783 (13)	0.413 (18)
O31	0.4803 (7)	0.4182 (14)	0.2013 (6)	0.302 (9)
O41	0.5039 (6)	0.5173 (12)	0.1128 (7)	0.234 (9)
C12	0.0073 (1)	0.5125 (2)	0.1682 (1)	0.0743 (9)
O12	0.0116 (7)	0.4625 (10)	0.1039 (6)	0.201 (7)
O22	0.0335 (7)	0.6359 (8)	0.1801 (6)	0.219 (7)
O32	0.0381 (6)	0.4387 (10)	0.2328 (6)	0.204 (7)
O42	−0.0807 (8)	0.5139 (10)	0.1498 (8)	0.229 (9)

Table 5. *Atomic positional and equivalent isotropic displacement parameters of* $[Fe(mtz)_6](BF_4)_2$ (*S4*) *at* 157 K

	x	*y*	*z*	*U* (Å²)
Fe1	0.0	0.0	0.0	0.0199 (4)
N411	0.0729 (3)	0.1177 (5)	−0.0432 (3)	0.0237 (19)
N311	0.1418 (3)	0.1854 (6)	0.0027 (3)	0.0330 (22)
N211	0.1821 (3)	0.2219 (6)	−0.0383 (3)	0.0389 (23)
N111	0.1381 (3)	0.1815 (5)	−0.1114 (3)	0.0272 (20)
C111	0.0723 (4)	0.1173 (6)	−0.1143 (3)	0.0256 (24)
C211	0.1629 (5)	0.2063 (9)	−0.1767 (4)	0.0500 (34)
N421	−0.0775 (3)	0.1661 (5)	−0.0041 (3)	0.0231 (19)
N321	−0.1316 (3)	0.1696 (6)	0.0320 (3)	0.0311 (22)
N221	−0.1705 (3)	0.2800 (6)	0.0169 (3)	0.0359 (23)
N121	−0.1441 (3)	0.3488 (5)	−0.0298 (3)	0.0269 (20)
C121	−0.0866 (4)	0.2787 (7)	−0.0399 (3)	0.0278 (25)
C221	−0.1723 (4)	0.4830 (7)	−0.0538 (4)	0.0389 (27)
N431	0.0823 (3)	0.0520 (5)	0.1225 (3)	0.0210 (18)
N331	0.1421 (3)	−0.0304 (5)	0.1711 (3)	0.0264 (19)
N231	0.1860 (3)	0.0314 (5)	0.2359 (3)	0.0293 (20)
N131	0.1547 (3)	0.1534 (5)	0.2292 (3)	0.0235 (19)
C131	0.0914 (4)	0.1642 (7)	0.1594 (3)	0.0250 (24)
C231	0.1889 (4)	0.2494 (7)	0.2928 (4)	0.0394 (28)
Fe2	0.5	0.0	0.0	0.0328 (5)
N412	0.4343 (3)	0.1236 (6)	−0.1011 (3)	0.0327 (22)
N312	0.3859 (3)	0.2269 (6)	−0.0991 (3)	0.0450 (26)
N212	0.3570 (3)	0.2856 (6)	−0.1653 (3)	0.0463 (26)
N112	0.3870 (3)	0.2256 (6)	−0.2116 (3)	0.0324 (22)
C122	0.4332 (4)	0.1275 (7)	−0.1721 (4)	0.0333 (27)
C212	0.3737 (4)	0.2771 (8)	−0.2899 (3)	0.0417 (29)
N422	0.5755 (3)	0.1667 (6)	0.0597 (3)	0.0352 (23)
N322	0.6219 (4)	0.1718 (7)	0.1389 (3)	0.0480 (27)
N222	0.6671 (4)	0.2767 (7)	0.1562 (3)	0.0484 (27)
N122	0.6519 (3)	0.3381 (5)	0.0882 (3)	0.0318 (22)
C122	0.5961 (4)	0.2718 (8)	0.0322 (4)	0.0376 (29)
C222	0.6952 (5)	0.4603 (7)	0.0875 (4)	0.0402 (30)
N432	0.4135 (3)	0.0469 (5)	0.0530 (3)	0.0316 (22)
N332	0.3604 (3)	−0.0448 (6)	0.0596 (3)	0.0434 (26)
N232	0.3216 (3)	0.0042 (6)	0.0996 (3)	0.0388 (22)
N132	0.3485 (3)	0.1288 (6)	0.1177 (3)	0.0277 (21)
C132	0.4041 (4)	0.1520 (7)	0.0884 (4)	0.0304 (27)
C232	0.3183 (4)	0.2086 (7)	0.1654 (4)	0.0354 (27)
B1	0.4521 (5)	0.5040 (10)	0.1485 (5)	0.0375 (31)
F11	0.3721 (3)	0.4725 (5)	0.1018 (2)	0.0747 (21)
F21	0.4582 (3)	0.6368 (5)	0.1442 (3)	0.0869 (25)
F31	0.4698 (3)	0.4712 (7)	0.2209 (3)	0.1211 (31)
F41	0.5011 (4)	0.4498 (8)	0.1203 (5)	0.1592 (48)
B2	−0.0041 (5)	0.5148 (10)	0.1633 (4)	0.0373 (32)
F12	0.0088 (3)	0.4484 (5)	0.1052 (2)	0.0680 (21)
F22	0.0217 (3)	0.6412 (5)	0.1685 (3)	0.0678 (23)
F32	0.0341 (3)	0.4519 (5)	0.2333 (3)	0.0723 (22)
F42	−0.0896 (3)	0.5159 (5)	0.1448 (3)	0.0716 (21)

sible and therefore both had to be used. The H positions were calculated and only the orientation of the terminal CH_3 group refined with a common isotropic displacement factor for the CH_3 group and a second U_{iso} for all other H atoms.

The intensity data of $[Fe(ptz)_6](BF_4)_2$ (*S2*) at 250 and 195 K were merged in $R\bar{3}$ and averaging of the three equivalents for all reflections resulted in internal *R* values of 2.8 and 3.3%, respectively. So the existence of the threefold axis is confirmed at least down to 195 K and the difficulties with other crystal samples already at this temperature have to be attributed to mechanical effects; for example, strains caused by different thermal expansion of crystal and adhesive resulting in deformations of the rather soft crystals. Structure refinement proceeded in a similar way as for 297 K, but with the exception that the difference electron density peaks around B indicated one preferred orientation of the BF_4 group, which was refined anisotropically without bond-length constraints. The starting values for all other atomic parameters were taken from the room-temperature structure. One common isotropic U_{iso} for all H atoms was refined. Positional parameters and equivalent isotropic displacements of all non-H atoms are listed in Table 3.

(*b*) Methyltetrazole compounds [(*S3*), (*S4*)]: The structure was solved by Patterson synthesis (Fe1 and Fe2 positions in $\bar{1}$) and subsequent electron density calculations by Fourier synthesis. In least-squares refinement the Fe positions were fixed at $\bar{1}$. The H positions were calculated with one common U_{iso} and

Table 6. *Atomic positional and equivalent isotropic displacement parameters of* $[Fe(mtz)_6](BF_4)_2$ (*S4*) *at* 113 K

	x	*y*	*z*	U (Å^2)
Fe1	0.0	0.0	0.0	0.0174 (4)
N411	0.0739 (2)	0.1170 (4)	−0.0426 (2)	0.0206 (16)
N311	0.1432 (3)	0.1847 (5)	−0.0028 (2)	0.0300 (18)
N211	0.1832 (3)	0.2221 (5)	−0.0383 (2)	0.0367 (20)
N111	0.1391 (2)	0.1787 (4)	−0.1117 (2)	0.0249 (17)
C111	0.0729 (3)	0.1157 (5)	−0.1142 (3)	0.0231 (20)
C211	0.1643 (4)	0.2045 (7)	−0.1768 (3)	0.0470 (28)
N421	−0.0772 (2)	0.1664 (4)	−0.0036 (2)	0.0210 (16)
N321	−0.1310 (3)	0.1720 (4)	0.0328 (2)	0.0273 (18)
N221	−0.1702 (3)	0.2817 (5)	0.0174 (2)	0.0309 (19)
N121	−0.1433 (2)	0.3510 (4)	−0.0295 (2)	0.0233 (16)
C121	−0.0863 (3)	0.2795 (5)	−0.0409 (3)	0.0232 (20)
C221	−0.1717 (3)	0.4844 (5)	−0.0542 (3)	0.0331 (22)
N431	0.0825 (2)	0.0521 (4)	0.1221 (2)	0.0182 (15)
N331	0.1426 (2)	−0.0304 (4)	0.1706 (2)	0.0236 (16)
N231	0.1866 (2)	0.0308 (4)	0.2357 (2)	0.0257 (17)
N131	0.1546 (2)	0.1523 (4)	0.2299 (2)	0.0217 (16)
C131	0.0907 (3)	0.1639 (5)	0.1593 (3)	0.0203 (19)
C231	0.1886 (3)	0.2504 (5)	0.2937 (3)	0.0311 (21)
Fe2	0.5	0.0	0.0	0.0287 (4)
N412	0.4342 (3)	0.1247 (4)	−0.1003 (2)	0.0284 (18)
N312	0.3878 (3)	0.2310 (5)	−0.0986 (3)	0.0385 (20)
N212	0.3593 (3)	0.2926 (5)	−0.1650 (3)	0.0390 (21)
N112	0.3874 (3)	0.2254 (5)	−0.2119 (2)	0.0295 (18)
C112	0.4326 (3)	0.1253 (6)	−0.1721 (3)	0.0302 (23)
C212	0.3743 (3)	0.2778 (6)	−0.2899 (3)	0.0357 (24)
N422	0.5764 (3)	0.1663 (5)	0.0602 (2)	0.0307 (19)
N322	0.6216 (3)	0.1719 (5)	0.1395 (3)	0.0413 (22)
N222	0.6683 (3)	0.2743 (5)	0.1573 (3)	0.0404 (21)
N122	0.6536 (3)	0.3392 (4)	0.0892 (2)	0.0271 (17)
C122	0.5974 (3)	0.2710 (6)	0.0322 (3)	0.0301 (22)
C222	0.6965 (4)	0.4605 (5)	0.0882 (3)	0.0339 (24)
N432	0.4127 (3)	0.0466 (4)	0.0524 (2)	0.0278 (18)
N332	0.3593 (3)	−0.0437 (5)	0.0588 (3)	0.0369 (20)
N232	0.3207 (3)	0.0046 (5)	0.0993 (2)	0.0320 (17)
N132	0.3489 (2)	0.1283 (5)	0.1187 (2)	0.0250 (17)
C132	0.4051 (3)	0.1525 (6)	0.0895 (3)	0.0285 (22)
C232	0.3192 (3)	0.2091 (6)	0.1663 (3)	0.0295 (22)
B1	0.4508 (4)	0.5069 (7)	0.1478 (3)	0.0309 (24)
F11	0.3703 (2)	0.4712 (4)	0.1009 (2)	0.0616 (16)
F21	0.4585 (2)	0.6381 (4)	0.1427 (2)	0.0607 (17)
F31	0.4672 (2)	0.4738 (5)	0.2223 (2)	0.0842 (20)
F41	0.5019 (3)	0.4439 (5)	0.1221 (3)	0.1181 (32)
B2	−0.0059 (4)	0.5174 (7)	0.1631 (3)	0.0290 (24)
F12	0.0087 (2)	0.4486 (3)	0.1053 (2)	0.0476 (15)
F22	0.0218 (2)	0.6437 (3)	0.1685 (2)	0.0484 (16)
F32	0.0343 (2)	0.4532 (3)	0.2344 (2)	0.0502 (15)
F42	−0.0909 (2)	0.5161 (4)	0.1448 (2)	0.0523 (15)

only the CH_3 rotations were refined. Positional parameters and equivalent isotropic displacements of all non-H atoms are listed in Tables 4–6.*

The rather high R values for all structures are considered to be due to the order–disorder phenomena.

Structure description

There are two different structure types, referred to, for convenience, as ptz and mtz structures. Common features are: molecular crystals are built up from centrosymmetric $[Fe(R\text{-}tz)_6]^{2+}$ complexes with a nearly ideal octahedral FeN_6 core and twice as many anions BF_4^- or ClO_4^-; these cations and anions are arranged in electrically neutral layers with (more or less) trigonal symmetry, linked together only by weak van der Waals forces; typical cation–anion distances within the layers are *ca* 6 Å, whereas the distances between the layers are *ca* 8 Å (mtz) and *ca* 11 Å (ptz); the cleavage planes of the crystals are parallel to these layers (*cf.* a projection of the unit cell perpendicular to the layers in Fig. 3).

Figs. 4(*a*) and 4(*b*) show *ORTEP* plots of 50% probability ellipsoids and the numbering scheme of the two inequivalent $[Fe(mtz)_6]^{2+}$ complexes, projected on the plane of the structural layers [(*S4*) at 157 K, representative for (*S3*) as well]. In the numbering scheme the first digit marks the atomic position within a ligand, the second digit numbers the three inequivalent ligands within each complex and the third digit distinguishes the two inequivalent complexes. The planar tetrazole rings make an angle of about 45° with the projection plane. The $[Fe(ptz)_6]^{2+}$ complex [(*S1*), (*S2*)] looks so similar, despite its higher symmetry, that an extra plot is superfluous; the numbering of atoms (only the first digit needed) corresponds to that of the mtz complex.

Main differences of the two structure types

(*a*) Propyltetrazole compounds: $[Fe(ptz)_6]X_2$ [X = BF_4 (*S2*), ClO_4 (*S1*)] crystallize in space group $R\bar{3}$ (hexagonal setting) with Fe in the special position 3(*a*): 0,0,0 (site symmetry $\bar{3}$) and all $[Fe(ptz)_6]^{2+}$ complexes are equivalent by lattice translations. All six ligands are equivalent according to the $\bar{3}$ symmetry. The anions are lying on the threefold axis, where B

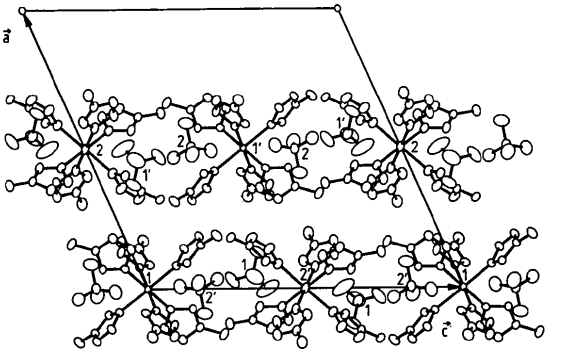

Fig. 3. Projection along the *b* axis of the complete unit-cell contents of $[Fe(mtz)_6](BF_4)_2$ (*S4*) at 157 K, clearly showing the layered structure. The numbers 1 and 2 mark the two inequivalent complex molecules and BF_4 groups, respectively. The centres of the groups with primed numbers are at a distance of *b*/2 above the projection plane.

* Lists of structure factors, anisotropic thermal parameters, H-atom parameters and a full list of distances and angles have been deposited with the British Library Document Supply Centre as Supplementary Publication No. SUP 55718 (82 pp.). Copies may be obtained through The Technical Editor, International Union of Crystallography, 5 Abbey Square, Chester CH1 2HU, England.

(or Cl, respectively) and one of the F (or O) atoms occupy the positions 6(*c*): 0,0,*z* and 0,0,$\bar{z}$ (site symmetry 3). The layers are perpendicular to the *c* axis and the network within the layers is exactly trigonal (Fig. 5*a*). Adjacent layers are shifted parallel to the planes according to the rhombohedral stacking (Fig. 6*a*). The stacking period is three.

(*b*) Methyltetrazole compounds: In $[Fe(mtz)_6]X_2$ [$X = BF_4$ (*S*4), ClO_4 (*S*3)] with space group $P2_1/n$ the most striking difference from the ptz structure is the existence of two inequivalent complexes [Fe1(mtz)$_6$] and [Fe2(mtz)$_6$] with Fe sites at the inversion centres 2(*a*): 0,0,0 and $\frac{1}{2},\frac{1}{2},\frac{1}{2}$ (Fe1) and 2(*b*): $\frac{1}{2}$,0,0 and 0,$\frac{1}{2},\frac{1}{2}$ (Fe2). There are three inequivalent ligands in each complex. The anions are in two different general positions. All complexes and anions are arranged in layers parallel to the *bc* planes (Fig. 5*b*). The monoclinic *b* and *c* axes correspond to the hexagonal [010] and [$\bar{2}$10] directions of the ptz structure (*cf.* Fig. 5*a*). Within the layers the pattern of cationic and anionic centres deviates only slightly from trigonal symmetry (~5% elongation of *c* with respect to $\sqrt{3}b$). The stacking period of these layers is two, where every second layer is rotated by 180° about the **b** direction, thus generating the twofold axis of the monoclinic structure which is missing in the rhombohedral ptz structure.

Within a layer the atomic positions of the two inequivalent complexes are related by a pseudo twofold screw axis parallel to the monoclinic *c* axis and passing through the point 0,$\frac{1}{4}$,0 as indicated in Fig. 5(*b*). But this screw axis is not compatible with the packing of the layers and consequently is not a symmetry element of the structure. The packing is shown in Fig. 6(*b*) which represents a section across the unit cell perpendicular to the layers and has to be compared with the corresponding picture of the ptz structure in Fig. 6(*a*). Nevertheless, it is possible to imagine two very different packings of these layers (produced by large relative shifts of the layers) which would allow for such a twofold screw axis and would have space groups *Pnma* or *Pbca*, respectively.

The lattice parameters vary linearly with temperature down to 110 K for the tetrafluoroborate [(*S*4), Fig. 2] and at least down to 160 K for the perchlorate [(*S*3), Fig. 1]. There is no hint of a phase transition. The *c* lattice constant (which is already larger than $\sqrt{3}b$ at room temperature) increases (BF_4) or remains constant (ClO_4) with decreasing temperature, whereas *b* decreases. This means that the deviation of the lattice from hexagonal metrics is growing on cooling.

So the mtz and ptz structures are rather similar, though there is no group–subgroup relation. The main differences involve twofold rotations of half of the molecules and some minor deformations. If bond distances and angles of the tetrazole rings are compared (Table 7), there are only small changes between the propyltetrazole and any of the inequivalent methyltetrazole ligands.

The geometrical similarity of the two inequivalent complexes as a whole is visualized in Fig. 7, where both are projected onto one another by the pseudo 2_1 axis. Moreover, the picture shows that the relative orientations of the ligands essentially do not change in the whole temperature range. Detailed data of the FeN_6 cores are given in Table 8. All Fe—N bond angles are very close to octahedral symmetry. There is no deviation from 90° larger than 2° at any temperature. The Fe—N bond distances are nearly equal for the three inequivalent N atoms only in complex 2, whereas in complex 1 the Fe—N411 bond is contracted but the Fe—N421 and Fe—N431 bonds are elongated. This octahedron is ortho-

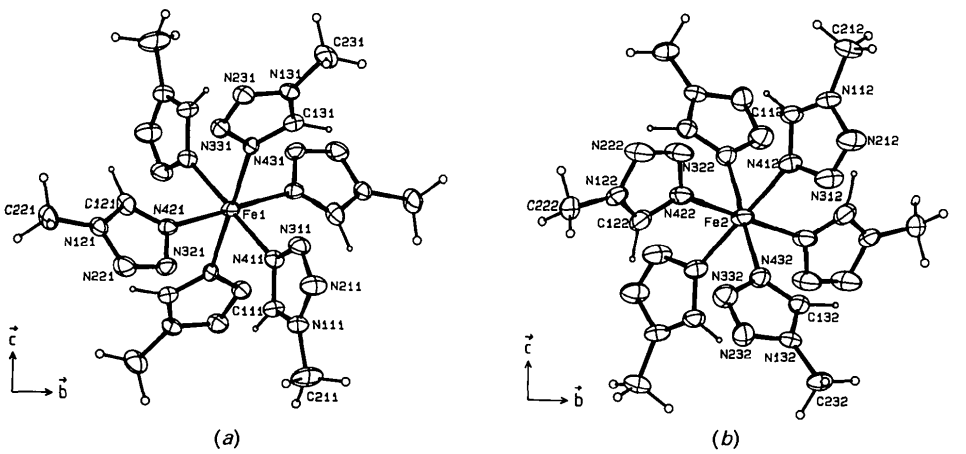

(*a*) (*b*)

Fig. 4. Complex molecules (*a*) [Fe1(mtz)$_6$] and (*b*) [Fe2(mtz)$_6$] of sample (*S*4) at 157 K, projected along the a^* axis, showing the 50% probability thermal ellipsoids and the nomenclature of the atoms. The different magnitudes of their ADP's are clearly seen.

rhombically distorted with nearly tetragonal symmetry. The changes of Fe—N bond lengths on cooling are somewhat different in the two complexes. For ligand No. 3 the bond distances increase on cooling and decrease only below 157 K, though in both complexes in a similar way. But for ligand No. 2 the temperature dependence in complex 1 is much steeper than in complex 2, thus changing the distortion of the Fe1 surrounding from a (nearly) axial compression along Fe1—N411 to a (nearly) axial

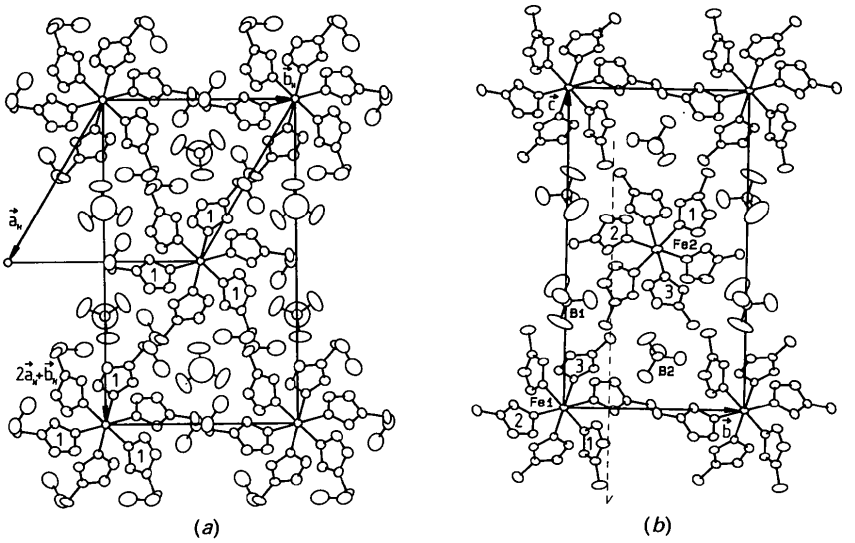

Fig. 5. (*a*) Projection along the threefold axis of $[Fe(ptz)_6](BF_4)_2$(*S*2) at 195 K. Included are only the cations and anions with centres exactly (Fe) or nearly (B) at zero height. The numbered ligands are above the projection plane and the others in centrosymmetric positions (Fe in $\bar{3}$) below the plane. A little more than the hexagonal cell is plotted for comparison with the mtz structure [*cf.* Fig. 5(*b*), which is drawn to the same scale]. (*b*) Projection along the a^* axis of $[Fe(mtz)_6](BF_4)_2$ (*S*4) at 157 K. Included are only the cations and anions with centres exactly (Fe1, Fe2) or nearly (B1, B2) at zero height. The three numbered inequivalent ligands are above the projection plane and the others in centrosymmetric positions (Fe in $\bar{1}$) below the plane. The atomic positions of the two inequivalent complexes are related by a pseudo-twofold screw axis along the *c* axis through the point $0,\frac{1}{4},0$ as indicated by the dotted line.

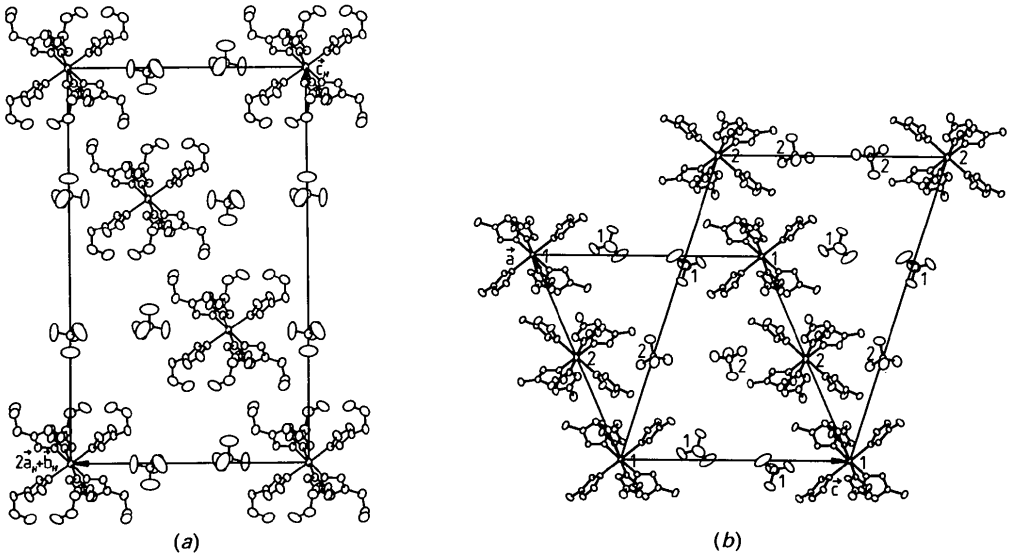

Fig. 6. (*a*) Projection along the hexagonal *b* axis of $[Fe(ptz)_6](BF_4)_2$ (*S*2) at 195 K, showing only the groups with centres at zero height. (*b*) Projection along the *b* axis of $[Fe(mtz)_6](BF_4)_2$ (*S*4) at 157 K, showing only the groups at zero height. For comparison with the analogous ptz plane in (*a*), an additional 'cell' has been drawn, which corresponds to the unit cell of the ptz structure.

Table 7. *Bond distances* (Å) *and angles* (°) *of the ligands: comparison between* $[Fe(mtz)_6](BF_4)_2$ (*S4*) *at* 157 K *and* $[Fe(ptz)_6](BF_4)_2$ (*S2*) *at* 195 K

	mtz						ptz
rg	11	21	31	12	22	32	
N(4*rg*)—N(3*rg*)	1.362 (6)	1.381 (9)	1.369 (6)	1.371 (9)	1.368 (7)	1.370 (9)	1.358 (4)
N(3*rg*)—N(2*rg*)	1.296 (9)	1.293 (8)	1.303 (6)	1.277 (8)	1.300 (9)	1.304 (10)	1.283 (5)
N(2*rg*)—N(1*rg*)	1.329 (7)	1.343 (9)	1.349 (7)	1.334 (9)	1.338 (8)	1.353 (8)	1.328 (3)
N(1*rg*)—C(1*rg*)	1.323 (9)	1.324 (9)	1.333 (6)	1.314 (8)	1.300 (8)	1.330 (10)	1.324 (5)
C(1*rg*)—N(4*rg*)	1.321 (9)	1.306 (8)	1.312 (8)	1.316 (9)	1.304 (10)	1.306 (9)	1.313 (4)
N(1*rg*)—C(2*rg*)	1.475 (11)	1.465 (8)	1.466 (8)	1.476 (9)	1.469 (9)	1.459 (10)	1.483 (5)
C(2)—C(3)							1.519 (6)
C(3)—C(4)							1.458 (9)
Fe(*g*)—N(4*rg*)—N(3*rg*)	125.0 (4)	124.2 (4)	122.9 (4)	123.1 (4)	123.9 (5)	121.7 (4)	123.8 (2)
Fe(*g*)—N(4*rg*)—C(1*rg*)	127.8 (4)	130.7 (5)	129.6 (4)	132.2 (5)	131.2 (4)	131.6 (5)	130.2 (2)
C(1*rg*)—N(4*rg*)—N(3*rg*)	105.6 (5)	105.1 (5)	107.1 (4)	104.5 (5)	104.4 (5)	106.4 (6)	106.0 (3)
N(4*rg*)—N(3*rg*)—N(2*rg*)	110.3 (5)	109.5 (5)	109.0 (5)	110.2 (6)	109.8 (6)	109.4 (5)	109.6 (2)
N(3*rg*)—N(2*rg*)—N(1*rg*)	106.2 (5)	107.5 (6)	107.0 (4)	107.4 (6)	106.6 (5)	106.8 (6)	107.6 (3)
N(2*rg*)—N(1*rg*)—C(1*rg*)	109.8 (6)	107.6 (5)	108.7 (5)	108.2 (6)	108.0 (6)	108.1 (6)	108.3 (3)
N(1*rg*)—C(1*rg*)—N(4*rg*)	108.1 (5)	110.3 (6)	108.3 (5)	109.6 (7)	111.0 (6)	109.2 (6)	108.5 (2)
N(2*rg*)—N(1*rg*)—C(2*rg*)	122.8 (5)	121.4 (6)	121.5 (4)	121.9 (6)	120.1 (5)	119.8 (6)	122.3 (3)
C(1*rg*)—N(1*rg*)—C(2*rg*)	127.4 (5)	130.6 (6)	129.8 (5)	129.6 (7)	131.9 (6)	132.0 (6)	129.2 (3)
N(1)—C(2)—C(3)							110.8 (4)
C(2)—C(3)—C(4)							114.0 (5)

Table 8. *Bond distances* (Å) *and angles* (°) *of the* FeN_6 *core*

	$[Fe(ptz)_6](ClO_4)_2$ (*S1*)	$[Fe(ptz)_6](BF_4)_2$ (*S2*)		
	299 K	297 K	250 K	195 K
Fe—N(4)	2.164 (4)	2.176 (4)	2.170 (4)	2.180 (3)
N(4)—Fe—N(4^i)	90.5 (1)	90.1 (1)	90.5 (1)	90.5 (1)
N(4)—Fe—N(4^{ii})	89.5 (1)	89.9 (1)	89.5 (1)	89.5 (1)

	$[Fe(mtz)_6](ClO_4)_2$ (*S3*)	$[Fe(mtz)_6](BF_4)_2$ (*S4*)	
	298 K	157 K	113 K
Fe(1)—N(411)	2.161 (6)	2.150 (6)	2.148 (5)
Fe(1)—N(421)	2.197 (5)	2.167 (5)	2.159 (4)
Fe(1)—N(431)	2.208 (4)	2.216 (4)	2.205 (3)
Fe(2)—N(412)	2.180 (5)	2.171 (5)	2.162 (4)
Fe(2)—N(422)	2.180 (6)	2.172 (5)	2.168 (4)
Fe(2)—N(432)	2.181 (8)	2.193 (6)	2.191 (5)
N(411)—Fe(1)—N(421^i)	88.7 (2)	88.8 (2)	88.5 (1)
N(421^i)—Fe(1)—N(431)	90.4 (2)	90.4 (2)	90.9 (1)
N(431)—Fe(1)—N(411)	90.9 (2)	90.3 (2)	90.2 (1)
N(411)—Fe(1)—N(421)	91.3 (2)	91.2 (2)	91.5 (2)
N(421)—Fe(1)—N(431)	89.6 (2)	89.6 (2)	89.1 (1)
N(431)—Fe(1)—N(411^i)	89.1 (2)	89.7 (2)	89.8 (1)
N(412)—Fe(2)—N(422^i)	90.4 (2)	90.6 (2)	90.6 (2)
N(422^i)—Fe(2)—N(432)	89.7 (2)	90.1 (2)	89.8 (2)
N(432)—Fe(2)—N(412)	91.0 (2)	92.0 (2)	91.8 (2)
N(412)—Fe(2)—N(422)	89.6 (2)	89.4 (2)	89.4 (2)
N(422)—Fe(2)—N(432)	90.3 (2)	89.9 (2)	90.2 (2)
N(432)—Fe(2)—N(412^i)	89.0 (2)	88.0 (2)	88.2 (2)

elongation along Fe1—N431. In the case of complex 2, which is almost ideally octahedral at room temperature, the changes on cooling result in an axial elongation along Fe2—N432.

A much more pronounced difference between the two inequivalent complexes $[Fe1(mtz)_6]$ and $[Fe2(mtz)_6]$ is found in their ADP's. These differences (*cf.* Table 9) are so large that they can directly be seen in the *ORTEP* plots (Figs. 4*a*, 4*b*). The differences between the ADP's of adjacent atoms within each complex are comparatively small. At room temperature, for example, the values of $U(Fe) - U(N)$ evaluated along the Fe—N bonds are between 0.001 and 0.004 Å^2 for both complex molecules, whereas the differences of the corresponding $U(Fe)$ values between the two complexes are about ten times larger: $U(Fe2) - U(Fe1)$ varies from 0.01 to 0.03 Å^2 in the three bond directions.

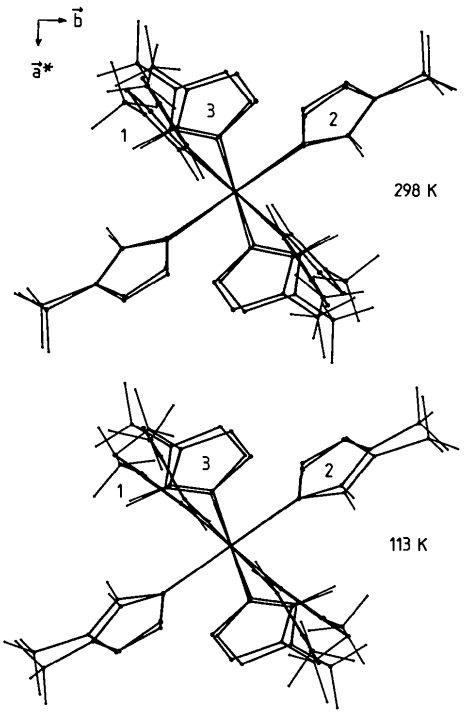

Fig. 7. Projection of the two $[Fe(mtz)_6]$ complexes along the *c* axis after rotation and translation of complex 2 about the pseudo-screw axis at 298 K (*S3*, top) and 113 K (*S4*, bottom).

Table 9. *Anisotropic ADP's of* Fe *in* $[Fe(R\text{-tz})_6]X_2$ ($X = ClO_4$, BF_4)

		U_{11}	U_{22}	U_{33}	U_{23}	U_{13}	U_{12}
(*S*1) ptz–ClO_4							
299 K	Fe	0.0374 (5)	0.0374 (5)	0.1026 (11)	0.0	0.0	0.0187 (3)
(*S*2) ptz–BF_4							
297 K	Fe	0.0359 (6)	0.0359 (6)	0.0659 (11)	0.0	0.0	0.0179 (3)
250 K	Fe	0.0304 (6)	0.0304 (6)	0.0590 (12)	0.0	0.0	0.0152 (3)
195 K	Fe	0.0225 (4)	0.0225 (4)	0.0404 (6)	0.0	0.0	0.0113 (2)
(*S*3) mtz–ClO_4							
298 K	Fe1	0.0469 (7)	0.0328 (6)	0.0347 (6)	−0.0001 (6)	0.0148 (5)	0.0023 (6)
	Fe2	0.0796 (10)	0.0587 (9)	0.0560 (8)	0.0000 (8)	0.0406 (7)	0.0040 (9)
(*S*4) mtz–BF_4							
157 K	Fe1	0.0204 (6)	0.0253 (8)	0.0140 (6)	0.0005 (7)	0.0068 (5)	0.0030 (7)
	Fe2	0.0377 (8)	0.0408 (9)	0.0272 (7)	−0.0033 (8)	0.0207 (6)	−0.0008 (9)
113 K	Fe1	0.0182 (5)	0.0222 (6)	0.0117 (5)	−0.0003 (5)	0.0060 (4)	0.0030 (6)
	Fe2	0.0353 (6)	0.0340 (7)	0.0245 (6)	−0.0052 (6)	0.0201 (5)	−0.0034 (7)

ADP's are affected by crystal quality, deficiencies of the structural model and other systematic errors like the effect of absorption or thermal diffuse scattering. The contribution of most of these errors to the ADP's, however, may in a first approximation be regarded as rather similar for all atoms of a structure (Chandrasekar & Bürgi, 1984) and thus should be of minor importance, if only differences of ADP's are considered. Therefore the difference of the ADP's between the two complexes is a more reliable result than the absolute values. The equivalent isotropic ADP's U_{iso}(Fe) of the two Fe sites are plotted as a function of temperature in Figs. 8 and 9, together with analogous data from Mössbauer measurements to be discussed later, and their differences $\Delta U_{iso} = U_{iso}(Fe2) - U_{iso}(Fe1)$ are shown in Fig. 10.

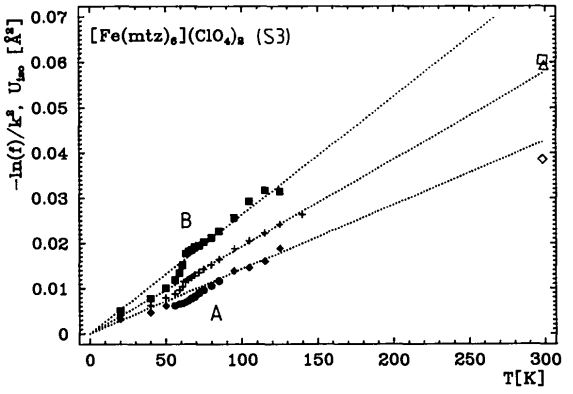

Fig. 8. Temperature dependence of the vibrational amplitudes of Fe in $[Fe(mtz)_6](ClO_4)_2$ (*S*3). U_{iso}(Fe2) (□) and U_{iso}(Fe1) (◇) are derived from structure determination at 298 K. The statistical errors do not exceed the height of the symbols. $\langle x^2 \rangle = -\ln(f)/k^2$ is derived from Mössbauer spectroscopy: the data points are (■) HS(*B*), (◆) HS(*A*) or LS(*A*), (●) the sum of HS(*A*) and LS(*A*) in the spin transition region, (+) the sum of all states. The dotted lines are linear regressions to the data points. Their slopes, in 10^{-4} Å^2 K^{-1}, are 1.42 (9) for site *A*, 2.62 (9) for site *B* and 1.93 (9) for the sum. Included is U_{iso}(Fe) (△) in $[Fe(ptz)_6](ClO_4)_2$ (*S*1) at 299 K.

The larger ADP's of complex 2 are correlated with a larger amount of space within the structure. Each Fe complex is surrounded by twelve anions, six in the same layer and three in each layer above and below. The distances from Fe to these anions are (at room temperature) about 6 Å with a spread of 0.3 Å for Fe1 as well as Fe2 within the layers, but range from 8.7 to 9.3 Å for Fe1 and from 9.5 to 10.1 Å for Fe2 between adjacent layers. This situation does not essentially change on cooling to 113 K.

A very similar situation has been found in $[Zn(mtz)_6](BF_4)_2$ and $[Cu(mtz)_6](BF_4)_2$ (Wijnands, 1989). These compounds are isomorphous to $[Fe(mtz)_6](BF_4)_2$ (*S*4) and $[Fe(mtz)_6](ClO_4)_2$ (*S*3) and have all significant structural features in common, especially the two inequivalent complex molecules with considerably different displacement parameters where the complex with the more octahedral $(Metal)N_6$ core has the larger ADP's. The equivalent isotropic values of the ADP's of Zn and Cu are

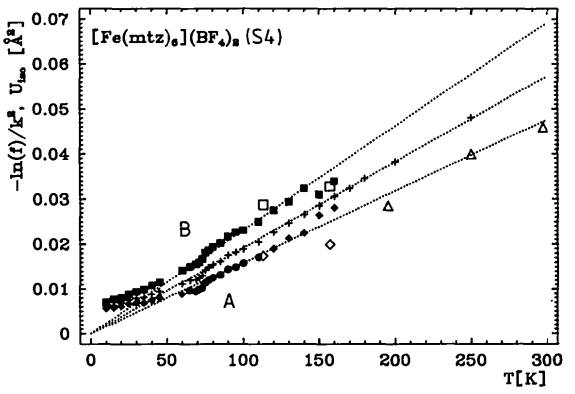

Fig. 9. Corresponding vibrational amplitudes in $[Fe(mtz)_6](BF_4)_2$ (*S*4). The meaning of the symbols is the same as in Fig. 8. The U_{iso} values from structure determination are at 157 and 113 K. The slopes of the fit curves are 1.59 (2) for *A*, 2.31 (2) for *B* and 1.91 (2) for the sum. Included are the values of U_{iso} (Fe) (△) in $[Fe(ptz)_6](BF_4)_2$ (*S*2) at 297, 250 and 195 K.

included in Fig. 10. They correspond well to the Fe data of (*S*3) and (*S*4). The relations between the six Zn—N distances in $[Zn(mtz)_6](BF_4)_2$ at 293 K are very similar to the analogous relations between the Fe—N distances in $[Fe(mtz)_6](ClO_4)_2$ (*S*3) at 298 K and the temperature variation of the relative Zn—N distances between 293 and 100 K is essentially the same as the temperature variation of the Fe—N distances comparing the perchlorate at 298 K (*S*3) with the tetrafluoroborate at 157 K (*S*4). The choice of anion seems to make no difference for these aspects of the mtz structure.

EPR measurements (Wijnands, 1989; Wijnands, Maaskant & Reedijk, 1986) of $[Zn(mtz)_6](BF_4)_2$ doped with Cu^{II} show at room temperature a superposition of two spectra, one isotropic and one anisotropic with axial symmetry. They are attributed to two CuN_6 sites, one in a dynamical Jahn–Teller state and the other static with axial distortion, where the dynamical Jahn–Teller state is correlated with the more octahedral Zn/Cu complex which has more space in the crystal structure. In the temperature range from 200 to 100 K the dynamic state changes into a static state too and only one axial spectrum is seen at 77 K. The copper ions behave differently according to the conditions provided by the two Zn lattice sites they occupy.

Relation to spin crossover

The essential impact of the HS→LS transition on the crystal structure comes from the volume contraction of the complex molecules by several per cent. The response of the structure to this contraction depends sensitively on the structural situation given in the HS state. On the other hand, this structural situation in the HS state determines whether the spin transition takes place at all. So the comparison of the two rather similar tetrazole structures with their markedly different spin transition behaviour was expected to reveal the main structural prerequesite for spin crossover to occur.

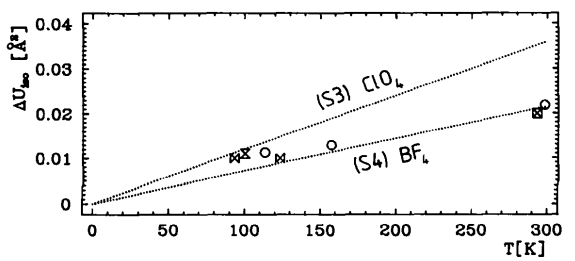

Fig. 10. Differences of the isotropic displacement factors U_{iso}(Fe2) − U_{iso}(Fe1), marked as circles, from $[Fe(mtz)_6](ClO_4)_2$ (*S*3) at 298 K and from $[Fe(mtz)_6](BF_4)_2$ (*S*4) at 157 and 113 K and the corresponding differences $\langle x^2\rangle(B) - \langle x^2\rangle(A)$ of the linear regressions of the Mössbauer data (dotted lines) for the perchlorate and the tetrafluoroborate. Additionally, the analogous U_{iso} differences from structure determinations by Wijnands are given for $[Zn(mtz)_6](BF_4)_2$ at 293 and 100 K (⊠) and for $[Cu(mtz)_6](BF_4)_2$ at 293, 123 and 93 K (⋈).

(*a*) In $[Fe(ptz)_6](BF_4)_2$ (*S*2) the spin transition causes a simultaneous structural phase transition (rhombohedral→triclinic) at 130 K, which has been characterized by powder diffractometry previously (Wiehl, Spiering, Gütlich & Knorr, 1990). Similar investigations were undertaken with the isomorphous mixed crystals $[Fe_xZn_{1-x}(ptz)_6](BF_4)_2$ (Schmitt, Wiehl, Knorr & Gütlich, in preparation). Zn, with its complete *d* shell, cannot show a spin transition and there is no structural phase transition in the mixed crystals with large Zn content (≥55%). As the ionic radius of Zn^{2+} (0.74 Å) is much closer to high-spin Fe^{2+} (0.76 Å) than to low-spin Fe^{2+} (0.58 Å) this fact corresponds to our understanding of the spin transition mechanism as being triggered by elastic interactions between large HS molecules and small LS molecules (Köhler, Jakobi, Meissner, Wiehl, Spiering & Gütlich, 1990). The knowledge of the crystal structure allows a microscopic interpretation of the measured lattice deformations accompanying the spin (and eventual structural phase) transition, as it is a question of crystal structure how the unit-cell contraction is distributed over the different directions in space. Details are given in the two papers cited above which describe the powder investigations. They also take account of other measurements which are beyond the scope of this paper.

(*b*) In the mtz compounds only one of the two inequivalent Fe complexes undergoes a spin transition. ^{57}Fe Mössbauer spectra of $[Fe(mtz)_6](BF_4)_2$ (*S*4) and $[Fe(mtz)_6](ClO_4)_2$ (*S*3) were measured by P. Poganiuch (Poganiuch, 1989; Poganiuch, Decurtins & Gütlich, 1990; Poganiuch & Gütlich, 1988). At room temperature these spectra show one quadrupole doublet typical to Fe^{2+} high spin. On cooling this doublet begins to split into two doublets at ~160 K for BF_4 and at ~130 K for ClO_4, indicative of the existence of two distinct Fe^{2+}(HS) sites designated *A* and *B*, which have to be attributed to the two inequivalent Fe lattice sites in the crystal structure. On further cooling the Fe complex at site *A* shows a complete HS→LS transition whereas the Fe complex at site B remains HS down to 5 K. The intensity ratio of the two sites is $A:B \simeq 1.5:1$ at the highest temperature where the two doublets are separated and changes continuously on cooling to 1:1 at 5 K.

The intensity of a quadrupole doublet (better: the effective thickness t_{eff} = constant × *nf* of the Mössbauer absorber) is proportional to the amount *n* of Fe and to the recoil free fraction (Lamb–Mössbauer factor) $f = \exp(-k^2\langle x^2\rangle)$, where $\langle x^2\rangle$ is the mean-

square vibrational amplitude of the Fe atom and $k = 2\pi/\lambda = 7.3$ Å^{-1} is the length of the wavevector of the 14.4 keV radiation of ^{57}Fe (Gonser, 1975). As the Lamb–Mössbauer factor f tends to nearly unity (apart from zero-point vibrations) at zero temperature the effective thickness at $T = 0$ K is determined by the Fe amount alone and an intensity ratio of 1:1 for sites A and B means equal amounts of Fe on these sites. Structure determination shows an Fe1:Fe2 ratio of 1:1 in the whole investigated temperature range of $113 < T < 298$ K. So the different Mössbauer intensities of A and B have to be attributed to different Lamb–Mössbauer factors $f(A) \neq f(B)$.

Comparison of Debye–Waller factors

The atomic displacement parameters of Fe1 and Fe2 will be compared with vibrational amplitudes $\langle x^2 \rangle$ for Fe(A) and Fe(B), which were derived from Mössbauer measurements under the condition that the abundances are $n(A) = n(B) = \frac{1}{2}$. In a diffraction experiment the Debye–Waller factor reduces the amplitude of the scattered wave by $f = \exp(-B\sin^2\theta/\lambda^2)$, where the isotropic atomic displacement parameter $U_{iso} = B/8\pi^2$ is interpreted, in the absence of static disorder, as the mean-square amplitude of the atomic motion. The corresponding quantity in Mössbauer spectroscopy is the Lamb–Mössbauer factor (Wilson, 1970) $f = \exp(-k^2\langle x^2 \rangle)$. As the Mössbauer effect operates on a time scale of about 10^{-7} s, which is slow compared to vibrational frequencies of the atoms it 'sees' the motion of the individual Fe nucleus. Details of the spectra depend on the electronic states, *i.e.* on the ligand field of Fe in its local chemical surrounding, but not on the distribution of Fe positions in space, as interference of waves plays no role. The resonantly absorbed intensities of the individual Fe atoms are simply summed up. So the Debye–Waller factors deduced from Mössbauer spectra are not affected by static disorder of the scattering atoms like the atomic displacement parameters from structure determination thus providing useful additional information.

The Debye–Waller factors $f(A)$, $f(B)$ and f(total) from Mössbauer measurements are plotted in Figs. 8 [($S3$), ClO_4] and 9 [($S4$), BF_4] in the form $-\ln(f)/k^2 = \langle x^2 \rangle$ as a function of temperature T. The values of f(total) stem from measurements of the total intensity of both doublets, which is the sum of the individual intensities on sites A and B, but is available even in a temperature range where the two doublets are not resolved. Only if the abundancies of the two sites are equal then $f(\text{total}) = [f(A) + f(B)]/2$. The validity of this relation was confirmed by the data which may be described quantitatively by the Debye model of the solid state. In this model the mean-square vibrational amplitudes are given as

$$\langle x^2 \rangle = \frac{3h^2T}{4\pi^2 k_B M \Theta^2} \left\{ \frac{T}{\Theta} \int_0^{\Theta/T} \frac{\xi \mathrm{d}\xi}{\exp(\xi) - 1} + \frac{\Theta}{4T} \right\}$$

(with Planck's constant h, Boltzmann's constant k_B, the vibrating mass M and the Debye temperature Θ). The expression in parentheses amounts to $\{...\} = \Theta/4T$ in the low-temperature limit $T \ll \Theta$ and is $\simeq 1$ for $T > \Theta$. The measured data $f(A)$, $f(B)$ and f(total) as function of temperature were fitted to straight lines simultaneously under the constraint: $f(\text{total}) = [f(A) + f(B)]/2$ at each temperature. For the fit only data above $\simeq 70$ K were used. The consistency of the fits (Figs. 8, 9) shows that the data can be explained by different Debye–Waller factors alone, without need of varying site populations. The differences $\langle x^2 \rangle(B) - \langle x^2 \rangle(A)$ of the linear regressions (no data points are given for clarity) are included in Fig. 10.

The slope of each curve is inversely proportional to $M\Theta^2$. So the Debye temperature Θ may be derived, if there is some idea about the vibrating mass M. This subject has been discussed earlier for other spin crossover compounds (Meissner, Köppen, Köhler, Spiering & Gütlich, 1987; Köppen, 1985). There the vibrating mass was estimated to be not the Fe mass, as has been used in several publications (König, Ritter, Kulshreshtha & Nelson, 1982), but rather the mass of the whole complex molecule, leading to Debye temperatures of the order of 50 K. This result is plausible, as the intramolecular forces are much stronger than the intermolecular forces and the molecules behave nearly as rigid bodies for lattice vibrations with wavelengths large compared to their dimensions.

With a mass of $M = 560$ a.m.u. for the [Fe(mtz)$_6$] complex the Debye temperatures were calculated as $\Theta = 36.9$ (1) K [$\Theta_A = 40.4$ (2), $\Theta_B = 33.5$ (2) K] for the tetrafluoroborate and $\Theta = 36.7$ (9) K [$\Theta_A = 42.7$ (14), $\Theta_B = 31.5$ (6) K] for the perchlorate. The order of magnitude is consistent with earlier results on other spin crossover compounds.

In the Mössbauer experiments only relative intensities were measured. So the logarithmic values plotted in Figs. 8 and 9 have an offset along the ordinate. Within the Debye model the theoretical value at $T = 0$ K is the zero-point vibration, whereas in the linear (high-temperature) approximation used here the value is zero. Consequently, the offset of the $\langle x^2 \rangle$ data in the plot was chosen such that the fitted lines pass through zero at $T = 0$ K. In the low-temperature region the data points deviate from the straight line according to the Debye law. They extrapolate to ~ 0.005 Å^2 at $T = 0$ K, which corresponds to the typical zero-point vibration of Fe.

The U_{iso} values of Fe1 and Fe2 are included in Figs. 8 ($S3$) and 9 ($S4$) for comparison. The vibra-

tional amplitudes of Fe from structure determination match those from Mössbauer measurements rather well, confirming that here indeed the atomic displacements are mainly caused by thermal vibration. The only exception is lattice site *B* for the mtz–ClO_4 structure (*S*3) at 298 K, where U_{iso}(Fe2) is smaller than the extrapolated value of $\langle x^2 \rangle(B)$. In both mtz compounds only Fe1/HS(*A*) undergoes an HS $\Longleftrightarrow$ LS transition at about 70 K. The complex on this lattice site has the smaller vibrations and the smaller distances to adjacent anions. It therefore experiences a higher pressure from its surroundings than complex 2/HS(*B*) and has a greater tendency to reduce its volume by changing into the LS state. Complex 2 on the contrary remains in the HS state on cooling to 4 K and may be converted into a metastable LS state only by irradiation with red light. So the vibrational amplitudes may be judged as a measure for the internal pressure of a complex and how likely it will give way to this pressure by an HS $\Longleftrightarrow$ LS transition.

This picture is supported by a comparison with the vibrational amplitudes of Fe in $[Fe(ptz)_6](BF_4)_2$ (*S*2). In this structure all Fe positions are equivalent and the compound undergoes a complete HS $\Longleftrightarrow$ LS transition at 130 K. The U_{iso}(Fe) values, which are included in Fig. 9, are comparatively small, much nearer to lattice site *A* than to site *B* of the mtz structure. $[Fe(ptz)_6](ClO_4)_2$ (*S*1) is isostructural to the tetrafluoroborate, only somewhat dilated because of the larger anion. The larger amount of space is in accordance with the larger vibrational amplitudes of the complex [*cf.* U_{iso}(Fe) in Fig. 8]. The structure seems to be rather unstable. All crystals investigated up to now cracked nearly explosively into small pieces in the temperature range of about 250 to 200 K. There is a spin transition at ~150 to 140 K, but preliminary powder diagrams (Schmitt, private communication) indicated that the crystal structure had already changed before the spin transition began.

There remains the question as to what makes up the difference of the two HS sites. A really astonishing result is that the two sites are not distinguishable in Mössbauer measurements above 160 K [BF_4, (*S*4)]. Not even a line broadening is detected, which would hint at a superposition of peaks. Only for the crystal structure is it clear that two states must already exist at room temperature.

The temperature dependence of lattice parameters gives no hint of a structural phase transition in the temperature region where the two HS doublets begin to separate. All significant structural differences between the two Fe complexes are essentially the same at room temperature as at 113 K. So they cannot be the reason for a property, which arises only below 160 K. The only structural feature that could be found to change considerably on cooling is the orientation of the thermal ellipsoids of Fe1 and Fe2. At room temperature their longest axes have directions essentially normal to the structural layers comparable to Zn1 and Zn2 (Wijnands, 1989). The relative orientations of the ellipsoids on the two inequivalent sites follow the twofold pseudosymmetry. For $[Zn(mtz)_6](BF_4)_2$ this situation does not change on cooling to 100 K. For $[Fe(mtz)_6](BF_4)_2$ (*S*4), in contrast, the longest principal axes of the Fe thermal ellipsoids make angles of about 60° with the normal on the layers at 157 K (where the two HS doublets begin to separate), retaining the pseudosymmetry between Fe1 and Fe2. At 113 K (where the two HS doublets are clearly separated) these angles are different for the two sites, $\simeq 60°$ (Fe1) and $\simeq 40°$ (Fe2).

I wish to express my sincere gratitude to Professor P. Gütlich for the years of good working conditions and the inspiring atmosphere in his group. My thanks to Professor M. Dräger and Dr G. Kiel are due to their generous disposal of measuring time on the four-circle diffractometer. I thank Dr P. Poganiuch for giving me his original Mössbauer results and Dr H. Spiering for many fruitful discussions. Financial support from the Deutsche Forschungsgemeinschaft and the Bundesministerium für Forschung und Technologie is greatly appreciated.

References

ADLER, P., WIEHL, L., MEISSNER, E., KÖHLER, C. P., SPIERING, H. & GÜTLICH, P. (1987). *J. Phys. Chem. Solids*, **48**, 517–525.

BUSING, W. R., MARTIN, K. O. & LEVY, H. A. (1964). *ORFFE*. Report ORNL-TM-306. Oak Ridge National Laboratory, Tennessee, USA.

CHANDRASEKAR, K. & BÜRGI, H.-B. (1984). *Acta Cryst.* B**40** 387–397.

CROMER, D. T. & LIBERMAN, D. J. (1970). *J. Chem. Phys.* **53**, 1891–1898.

CROMER, D. T. & MANN, J. B. (1968). *Acta Cryst.* A**24**, 321–324.

DECURTINS, S., GÜTLICH, P., HASSELBACH, K. M., HAUSER, A. & SPIERING, H. (1985). *Inorg. Chem.* **24**, 2174–2178.

DECURTINS, S., GÜTLICH, P., KÖHLER, C. P. & SPIERING, H. (1985). *Chem. Commun.* pp. 430–432.

DECURTINS, S., GÜTLICH, P., KÖHLER, C. P., SPIERING, H. & HAUSER, A. (1984). *Chem. Phys. Lett.* **105**, pp. 1–4.

DOYLE, P. A. & TURNER, P. S. (1968). *Acta Cryst.* A**24**, 390–397.

FRANKE, P. L. (1982). *Tetrazoles in Coordination Chemistry*. PhD Thesis, Univ. Leiden, The Netherlands.

FRANKE, P. L. & GROENEVELD, W. L. (1981). *Transition-Met. Chem.* **6**, 54–56.

FRANKE, P. L., HAASNOOT, J. G. & ZUUR, A. P. (1982). *Inorg. Chim. Acta*, **59**, 5–9.

GONSER, U. (1975). *Topics in Applied Physics*, Vol. 5, *Mössbauer Spectroscopy*. Berlin: Springer.

JOHNSON, C. K. (1966). *ORTEP*. Report ORNL-3794, revised. Oak Ridge National Laboratory, Tennessee, USA.

KAMIYA, T. & SAITO, Y. (1971). German Patent P2147023.5.

KÖHLER, C. P., JAKOBI, R., MEISSNER, E., WIEHL, L., SPIERING, H. & GÜTLICH, P. (1990). *J. Phys. Chem. Solids*, **51**, 239–247.

KÖNIG, E. (1987). *Prog. Inorg. Chem.* **35**, 527–622.
KÖNIG, E., RITTER, G., KULSHRESHTHA, S. K. & NELSON, S. M. (1982). *Inorg. Chem.* **21**, 3022–3029.
KÖPPEN, H. (1985). *Der Isotopeneinfluß auf den Spinübergang im System* [Fe(2-pic)$_3$]Cl$_2$.Sol (Sol = EtOH, MeOH). PhD Thesis, Univ. Mainz, Germany.
MCCANDLISH, L. E., STOUT, G. H. & ANDREWS, L. C. (1975). *Acta Cryst.* A**31**, 245–249.
MEISSNER, E., KÖPPEN, H., KÖHLER, C. P., SPIERING, H. & GÜTLICH, P. (1987). *Hyperfine Interact.* **36**, 1–12.
MEISSNER, E., KÖPPEN, H., SPIERING, H. & GÜTLICH, P. (1983). *Chem. Phys. Lett.* **95**, pp. 163–166.
MÜLLER, E. W., ENSLING, J., SPIERING, H. & GÜTLICH, P. (1983). *Inorg. Chem.* **22**, 2074–2078.
POGANIUCH, P. (1989). *Untersuchung des thermisch- und lichtinduzierten Spinüberganges in Eisen*(II)*-Komplexen des Typs* [Fe(1-*Methyl*-1*H*-*tetrazol*)$_6$]X_2 (X = BF_4^-, ClO_4^-, PF_6^-, $CF_3SO_3^-$). PhD Thesis, Univ. Mainz, Germany.
POGANIUCH, P., DECURTINS, S. & GÜTLICH, P. (1990). *J. Am. Chem. Soc.* **112**, 3270–3278.
POGANIUCH, P. & GÜTLICH, P. (1987). *Inorg. Chem.* **26**, 455–458.
POGANIUCH, P. & GÜTLICH, P. (1988). *Hyperfine Interact.* **40**, 331–334.
SHELDRICK, G. M. (1976). *SHELX*76. Program for crystal structure determination. Univ. of Cambridge, England.
SPIERING, H., MEISSNER, E., KÖPPEN, H., MÜLLER, E. W. & GÜTLICH, P. (1982). *Chem. Phys.* **68**, 65–71.
SPIERING, H. & WILLENBACHER, N. (1989). *J. Phys. Condens. Matter* **1**, 10089–10105.
WIEHL, L., KIEL, G., KÖHLER, C. P., SPIERING, H. & GÜTLICH, P. (1986). *Inorg. Chem.* **25**, 1565–1571.
WIEHL, L., SPIERING, H., GÜTLICH, P. & KNORR, K. (1990). *J. Appl. Cryst.* **23**, 151–160.
WIJNANDS, P. E. M. (1989) *The Jahn–Teller Effect in Crystals of Hexacoordinated Copper*(II) *Complexes*. PhD Thesis, Univ. Leiden, The Netherlands.
WIJNANDS, P. E. M., MAASKANT, W. J. A. & REEDIJK, J. (1986). *Chem. Phys. Lett.* **130**, pp. 536–540.
WILLENBACHER, N. & SPIERING, H. (1988). *J. Phys. C*, **21**, 1423–1439.
WILSON, A. J. C. (1970). *Elements of X-ray Crystallography* . New York: Addison-Wesley.

Acta Cryst. (1993). B**49**, 303–309

A Study of Two Polymorphic Modifications of (*S*)-1-Phenylethylammonium (*S*)-Mandelate and the Structural Features of Diastereomeric Mandelate Salts

BY SINE LARSEN AND HEIDI LOPEZ DE DIEGO

Department of Chemistry, University of Copenhagen, The H. C. Ørsted Institute, Universitetsparken 5, *DK*-2100 *Copenhagen Ø, Denmark*

(*Received* 21 *April* 1992; *accepted* 7 *July* 1992)

Abstract

A low-temperature modification of (*S*)-1-phenylethylammonium (*S*)-mandelate has been investigated: $C_8H_{12}N^+.C_8H_7O_3^-$, $M_r = 273.33$, monoclinic, $P2_1$, $a = 8.322$ (4), $b = 6.801$ (2), $c = 12.885$ (3) Å, $\beta = 91.74$ (3)°, $V = 728.9$ (8) Å^3, $Z = 2$, $D_x = 1.245$ g cm^{-3}, λ(Cu $K\alpha$) = 1.5418 Å, $\mu = 6.60$ cm^{-1}, $F(000) = 292$, $T = 122.0$ (5) K, $R = 0.044$ for 1571 observed reflections. In this polymorph both the stereochemistry of the ions and their hydrogen bonding are identical to the orthorhombic modification obtained at 298 K. An analysis of 23 different mandelate stuctures showed the existence of a preferred conformation of the mandelate ion with an almost planar arrangement of the carboxy and the hydroxy groups. The hydrogen bonding in the mandelates is described by graph theory. This shows that, although a single common motif is not observed in all the mandelate structures, chains of hydrogen bonds are found in all the mandelates of primary and secondary amines.

Introduction

A very common method of separating a racemic mixture into its enantiomers is through the formation of diastereomeric compounds by reaction with an optically active compound. If the difference in their solubilities is sufficiently large, a separation of the enantiomers may be achieved. For an understanding of the differences between the physicochemical properties of the diastereomeric salts, knowledge of their crystal structure is of great significance. As for other compounds, different polymorphic modifications may exist for the diastereomeric salts. Interactions between chiral molecules should be common in polymorphic structures and it seems plausible that the structural differences between polymorphic modifications are related to differences in the interactions between chiral entities.

Mandelic acid is widely used as a resolving agent for the resolution of racemic amines and has been used to resolve 1-phenylethylamine (Larsen & Lopez de Diego, 1992). In our investigations of the dia-

0108-7681/93/020303-07$06.00